The Eyre Peninsula conductivity anomaly, South Australia

Thesis submitted in accordance with the requirements of the University of Adelaide for an Honours Degree in Geophysics

Lachlan   Loader

April   2019

THE UNIVERSITY
of ADELAIDE

THE EYRE PENINSULA CONDUCTIVITY ANOMALY, SOUTH AUSTRALIA

EYRE PENINSULA CONDUCTIVITY ANOMALY

ABSTRACT

A major electrically conducting structure has been spatially located in the southern Eyre Peninsula, South Australia. The structure extends from the continental margin inland along the eastern margin of the Eyre Peninsula, trending north-northeast for approximately 150 km. In order to provide a two-dimensional image of the crust orthogonal to the conductor's strike, 39 broadband (1000 to 0.01 Hz) magnetotelluric sites were collected with approximately 2 km separation across the peninsula. A smoothed 2-D inversion model demonstrated that the conductor appears centred beneath a topographic high, structurally bound at the east by the transpressional Kalinjala Shear Zone and resistive Donington Suite granitoids, and the Sleaford Complex to the west. The main features from modelling are: (i) east of the Kalinjala Shear Zone, a region of high resistivity (> 1000 ohm/m) relates to the Donington Suite granitoids; (ii) the late Archaean Sleaford Complex (2480–2420 Ma) bordering the Donington Suite granitoids features a lower, wider resistivity range between 5 to < 600 ohm/m, and is near-vertical in the top 12 km; (iii) the lowest resistivity structure of < 0.1 ohm/m occurs at a depth of 5-10 km, and appears to terminate at a depth of ~15 km. The low resistivity structure correlates with banded iron formations, and is credibly the result of biogenically deposited graphite in marine sediments, which migrated to become concentrated in fold hinges during the Kimban Orogeny; and (iv) the conductor is collocated with a ridge of high gravity (+ 200 to 500 mGals). The origin of this high gravity may be due to a mafic intrusive block of oceanic crust, compressed during the continental collision of the Kimban Orogeny. Utilising the constraints of the 2-D model, a regional 3-D forward model was developed which shows agreement with compiled legacy data sets.

KEYWORDS

TABLE OF CONTENTS

LIST OF FIGURES AND TABLES

INTRODUCTION

Over 40 years ago, White and Milligan (1984) conducted an EM induction study in the Eyre Peninsula, which forms the southern portion of the Gawler Craton in South Australia. White and Milligan's intention was to study the effect of coastal disturbance, hoping to discover a cause of the coast effect observed by White and Hopgood (1979). This study revealed an expansive, highly electrically conducting structure located in the region. At the time, the supposition was that this conductivity anomaly was caused by current channelling from the ocean into the upper crust, as the electrical conductance was higher than that of the deep ocean (and among the world's most conductive features). One of the unique properties of this structure was that it appeared to have no coincident surface structure with which it might be associated (White and Milligan, 1984). This discovery spawned 40 years of research into the so-named Eyre Peninsula conductivity anomaly (EPCA) (White & Milligan, 1984, 1986; White and Polatajko, 1985; Milligan *et al*., 1989; Kusi *et al*., 1998; Popkov *et al*., 2000; Thiel *et al*., 2005). The EPCA is located in the southern Gawler Craton, and is parallel to the magnetic lineations formed by banded iron formations in the Hutchison metasediments (Thiel, 2005). The surface layer of the EPCA is comprised of Hutchison Group metasediments which formed between 2000–1850 Ma, which increase in thickness towards the east (Parker *et al*., 1988). This region of the Gawler Craton was heavily affected by the Kimban Orogeny (1730-1690 Ma) which severely deformed several units of rocks in the area (Parker and Lemon, 1982; Hand, 2007).

Legacy data for the project was collated in order to model regional trends, with legacy data referring to all historic magnetotelluric and geomagnetic datasets collected pertaining to the Eyre Peninsula conductivity anomaly, totalling 226 sites. Two-

dimensional modelling of legacy data to constrain the EPCA estimated its maximum

depth at 15 km. Legacy data is extensive in the region, with two surveys (Kusi *et al*.,

1998; Popkov *et al*., 2000) exploring a wide north-south boundary to examine the shape

and extent of the EPCA. A 2-D thin sheet model used to interpret geomagnetic depth

sounding (GDS) data (Kusi *et al*., 1998) demonstrates a decrease of conductivity inland,

with the EPCA terminating approximately 140 km north of the southern cape.

Earthquakes exceeding magnitude 4 in the region occur predominantly to the west of

the EPCA (Kusi *et al*., 1998). Previous electromagnetic spatial analyses from legacy

data have connected the conductivity anomaly to a Mesoproterozoic crustal mechanism;

however, due to these studies' low sampling rate and limitations in bandwidth, little

could be said about the depth and dimensions of the conductor, hence the geological

relation is ambiguous.

Modelling the legacy data as a series of regional maps depicting gravity, elevation,

magnetic lineation and induction arrows indicates a broadly two-dimensional

conductivity structure, leading to the development of transect TB2018: a broadband

(1000 to 0.01 Hz) magnetotelluric survey running east-west perpendicular to the EPCA,

featuring dense 2 km spacing in order to resolve depths up to 50 km with high fidelity.

This research aims to bridge the gaps in knowledge pertaining to the EPCA, refining our

understanding of its potential origins, dimensions, and geological associations.
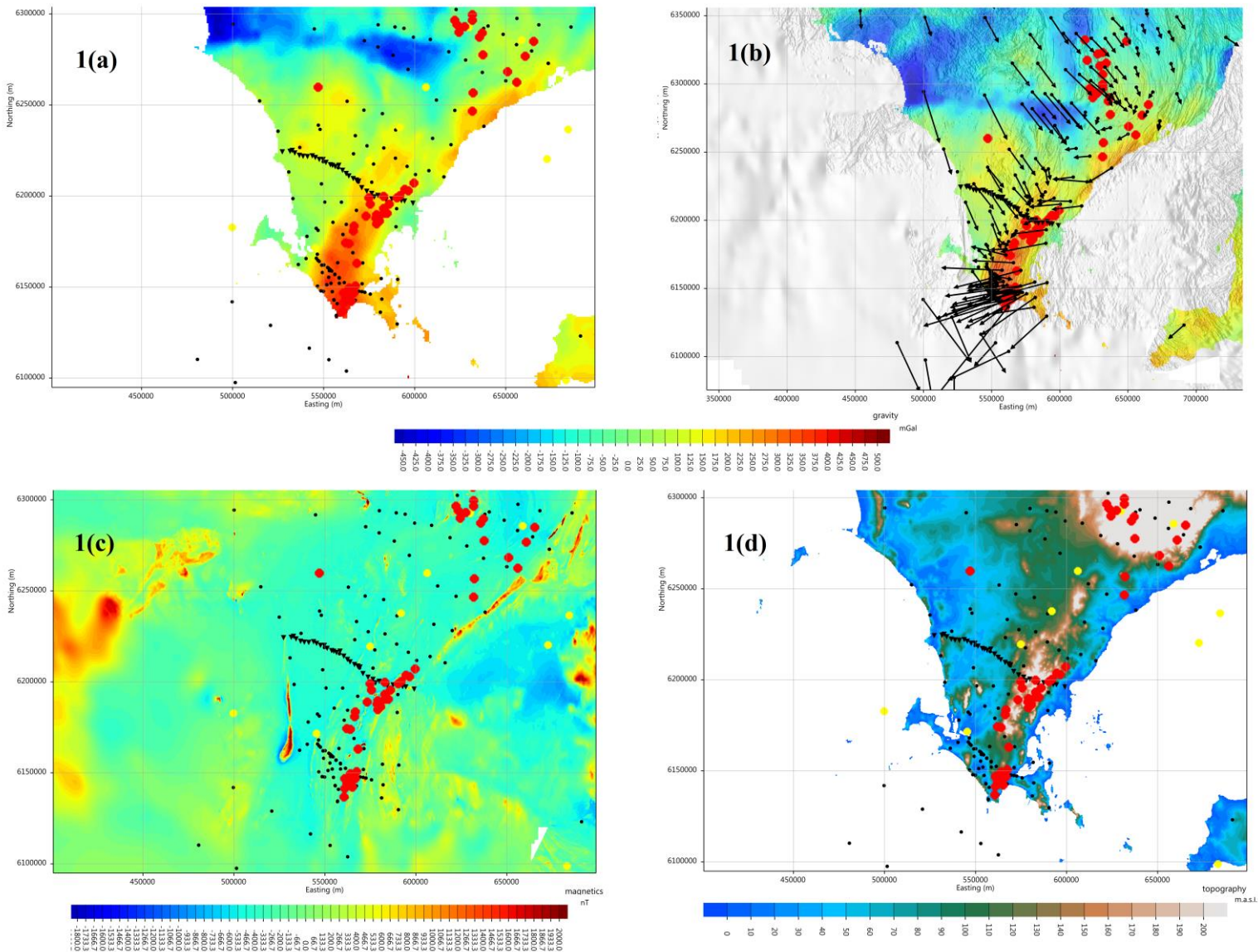
Figure 1: Regional maps of the southern Eyre Peninsula compiled from legacy data sets, displaying from top left to bottom right: 1(a) gravity, 1(b) Parkinson induction arrows constructed at 1000 s overlain on regional gravity, 1(c) magnetic lineations, and 1(d) elevation. Each base map was created using GeoTools, and is geographically referenced to the UTM coordinate system. TB2018 profile line is indicated by the inverted black triangles, and runs approximately perpendicular to the EPCA and the Kalinjala shear zone (Thiel *et al*., 2005). Red circles represent graphite occurrences across the Eyre Peninsula, yellow circles indicate available earthquake data exceeding magnitude 4. Small black circles are the locations of previous geomagnetic and magnetotelluric study sites.

GEOLOGICAL SETTING

The Eyre Peninsula comprises a segment of the Gawler Craton, a large, polygonal tectonic unit which forms part of the stratotectonic, late Archaean (2550–2500 Ma) to middle Proterozoic (2000-1690 Ma) Central Australia geological province (tectonic map of Australia and New Guinea, Rutland *et al.*, 1981; Parker *et al.*, 1993). The Delamerian Fold Belt defines the north-eastern and eastern boundaries of the Gawler Craton, inclusive of the 40 km extent of the Torrens Hinge transition zone (Kusi, 1998). The south-western boundary of the Gawler Craton is defined by a rift complex which formed during the Mesozoic separation of Australia from Antarctica (~95 Ma (Veevers, 1986)). There is contention over the definitions of the western and north-western boundaries, With Parker (1980) suggesting that the Musgrave orogenic domain and thickening sediments of the Officer Basin define the north-western boundary, and the eastern edge of the Eucla basin defining the western boundary. Conversely, Webb *et al.* (1986) proposes the boundaries are unable to be defined due to superficial cover.

The Gawler Craton can be approximated as a series of tectonic subdomains, based on metamorphic, stratigraphic and structural character. While four distinctions are possible - those being the Coulta Subdomain (Thomson, 1980), the Cleve Subdomain, the Gawler Ranges Middle Proterozoic volcanic province (Giles, 1977; Branch, 1978), and the Stuart Shelf Adelaidean sedimentary province (Sprigg, 1952; Manson *et al.*, 1978) - for the purposes of this research, the discussion of tectonism will be limited to the Coulta and Cleve subdomains.

The Coulta Subdomain consists of remnants of Archaean to Proterozoic basement rock (Thomson, 1980, Kusi *et al.,* 1998). It is defined by an absence of Proterozoic intrusives, metasediments or volcanics, and is comprised of gneissic and granitic rock.

The basement formed during the Sleafordian Orogeny (2480–2420 Ma) in the late Archaean (Hand, 2007), and is thus called the Sleaford Complex. Counter to this, the Sleaford Complex extends into the Cleve Subdomain, but is uncomfortably overlain by sediments, and contains a considerable volume of young intrusives and supracrustal sequences.

The Cleve Subdomain comprises two parallel zones, henceforth referred to as zones 2a (the western zone) and 2b (the eastern zone). Zone 2a comprises an early to mid-Proterozoic mobile zone containing highly deformed and metamorphosed sediments, called the Hutchison Group (Vassallo and Wilson, 2002; Hand, 2007). The Hutchison Group sediments were deformed through several episodes of folding, emplacement, and granulite-facies metamorphism (Parker and Lemon, 1982) creating a series of inhomogeneous, elongated dome-and-basin shaped structures which trend northeast-southwest, with north-south rotation the further north the zone extends (Parker and Lemon, 1982). Parker *et al*. (1988) proposed that as the Sleafordian basement developed, shallow-water shelf sediments were uncomfortably overlain on top of them, forming the Hutchison metasediments. The top of the Hutchison Group is comprised of a psammopelitic schist, the Yadnarie Schist. Below this is the Middleback Subgroup, containing typical carbonate, pelitic and iron-ore hosting iron formations. The basal unit is a sequence of mixed chemical and classic sediments, the Warrow Quartzite, an expansive cross-bedded unit, interbedded with dolomite (Parker and Lemon, 1982; Hand, 2007).

A graphitic schist extends along the east coast from Sleaford Bay to the north of the Eyre Peninsula, held within the Middleback Subgroup, just above the Warrow Quartzite. On a local scale, enrichment of graphite has expressed as economic-grade

concentrations, mined in two locations; Koppio, 2 km west of Tumby Bay, and Uley, a mine 10 km northwest of Sleaford Bay. Through modelling, it can be inferred that the graphitic schists form a near-continuous band at the base of the Hutchison Group, with Johns (1961) supposing that a haematite-quartzite formation occurs at approximately the same depth and relief as the graphitic schist, sometimes interbedded or cross-cutting the graphitic schist. Graphite is also present in graphite quartz-feldspar-garnet-biotite gneisses, which form distinct stratigraphic units in the Hutchison Group.

The Kimban Orogeny (1730-1690 Ma) saw the formation of complex gneisses in the south-east Eyre Peninsula (Hand, 2007). The Cornian-aged structural fabrics, separated from the Hutchison Group in the east by a north-trending mylonite zone (Rutland *et al*., 1981) are contrasted with Zone 2b in the east, which is characterised by less intense deformation and metamorphic acid-sourced volcanics. Both zones consist of Middle Proterozoic undeformed clastic sediments overlying metamorphosed sequences. Before the Kimban Orogeny, the Cornian (previously Lincoln) Orogeny compressional event around 1850 Ma occurred, folding the Hutchison Group (Parker, 1993; Vassallo & Wilson 2002). As a result of this event, granitoids in the east were emplaced, forming the Donington Suite granitoids. After this compressional event, an extensional event produced Tournefort dykes striking north-south, featuring magmatic sub-basins which may have developed in a continental-interior setting (Schwarz, 2002; Thiel *et al*., 2005). Following this extension, the Kimban Orogeny reworked a large portion of the Hutchison Group, resulting in anticline and syncline formation within the Hutchison metasediments.
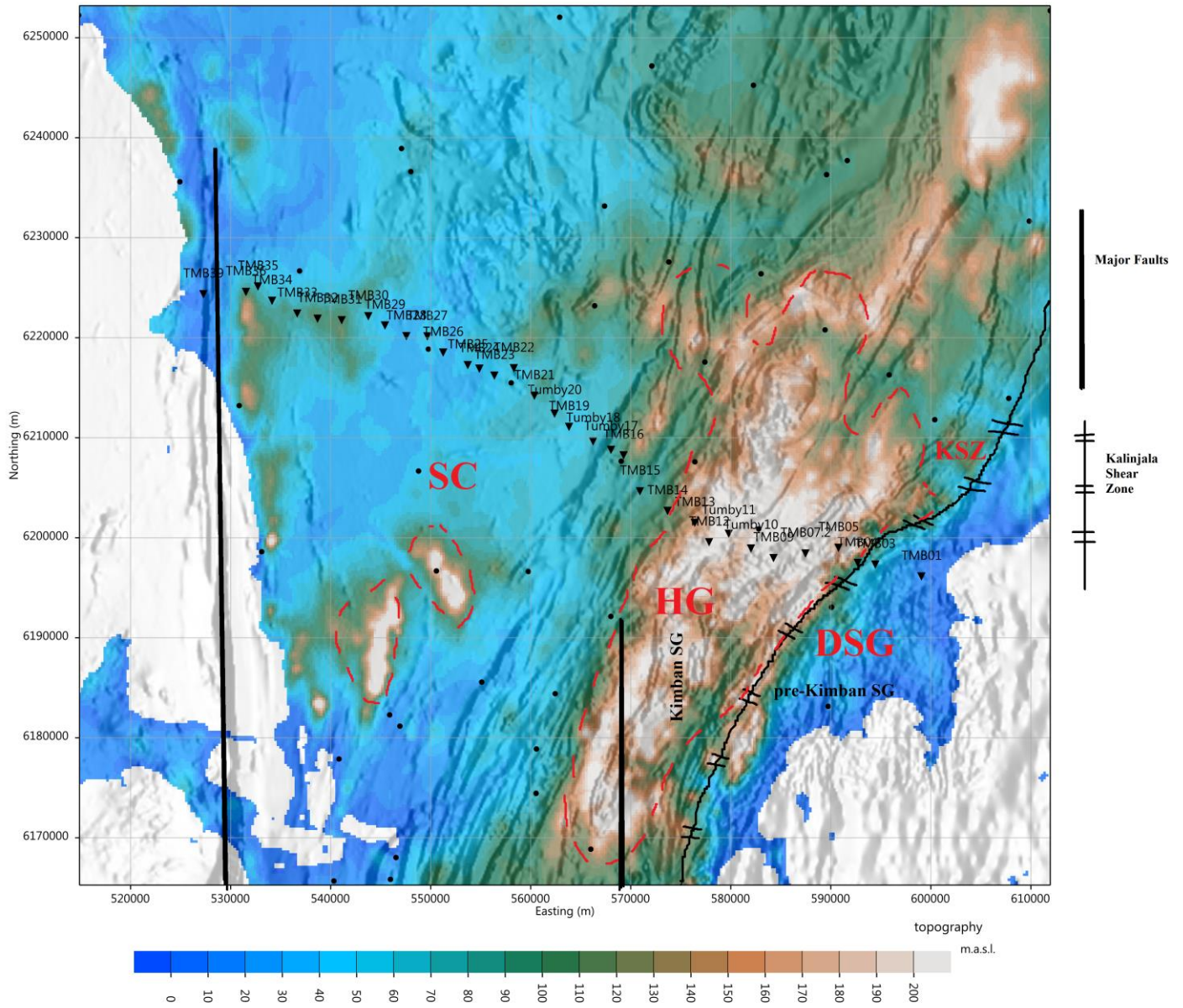
Figure 2: **South-east Eyre Peninsula, signifying the 1730 to 1690 Ma Kimban Orogeny and the resultant geological and topographic impacts. DSG = Donington Suite granitoids, HG = Hutchison Group, KSZ = Kalinjala Shear Zone, SC = Sleaford Complex. Topography indicated in metres above sea level (m.a.s.l.). Total magnetic intensity (TMI) image of the south-east Eyre Peninsula, South Australia. TMI image expresses the Donington Suite, Hutchison Group, Kalinjala Shear Zone and Sleaford Complex. Rotated into the Kalinjala shear zone are pre-Kimban Orogeny structural fabrics (pre-Kimban SG) preserved in banded iron formations.**

One of the foremost expressions of the Kimban Orogeny tectonism was the dextral transpression which resulted in the Kalinjala Shear Zone (KSZ) out of a growth fault. The KSZ forms a high-strain zone between 4 and 6 km wide along the east coast of the Eyre Peninsula (Figure 2; Parker 1980; Vassallo and Wilson, 2002; Hand, 2007). The zone also features deformation and metamorphism within the KSZ, between 50 and 100 km of width, preserving chevron folding and noncylindrical folding (Vassallo and Wilson, 2002), with granulite-facies mineral assemblages (Hand, 2007).

SURVEY

The magnetotelluric survey TB2018 was conducted along an 80 km east-west transect across the Eyre Peninsula. The survey involved the deployment of 39 broadband stations, spaced at intervals of 2 km, the data was collected between the 18th and 25th of July 2018 in South Australia. The station identified with the least noise was at the western-most end of the transect, this site becoming the location of the remote reference. The magnetic components (Bx and By), and the electric components (Ex and Ey) were recorded at each station for an approximate period of 48 hours, with leeway permitting access issues and weather inclemency. The devices used were Lemi-423 broadband magnetotelluric instruments, which were oriented to local geomagnetic coordinates, and later rotated to geographic coordinates. Instruments sampled at a rate of 1000 Hz, and all recordings were synchronised by the on-board GPS in order to improve the efficacy of the remote reference during data processing.

A grounding electrode was installed at each site. The electrode is composed of solid brass, and hammered into earth within the boundaries of the dipoles.

The eletrodes deployed were Cu-CuSO$_4$ Lemi-701 apparatuses, oriented to magnetic north-south and east-west. Lemi logging software records the electric field in uV/m. Electrodes are buried vertically, at a depth sufficient to cover them completely. A firm deployment is essential to reduce disturbance which may result in noisy data.

The magnetic field recorded in its induction components Bx and By, was recorded utilising Lemi-120 magnetometers, spaced 5m apart and oriented parallel to the electric dipoles. The induction coils recorded in a frequency range between 10^{-3} and 10^3 Hz. At each station, the data window was assessed visually on the quality and precision of the phase and apparent resistivity plots. It is readily apparent when there has been an issue with the deployment, such as improperly installed electrodes or a magnetometer which is not recording a signal, and is able to be fixed on site. Lemi-423 logging devices produce one-and-a-half-hour data files, saved to SD cards as an encrypted data file.

DATA PROCESSING

In processing the magnetotelluric data, four programs were utilised, two of which were supplied by LEMI Software: Lemigraph and Lemi423 Processing software. WinGLink geophysical modelling software was used for further refinement after the initial stages of processing, and Geotools, an open source GIS toolkit used for enhanced regional data interpretation functionality.

Data were converted into ASCII format from their encrypted data files utilising Lemi423, after which each hour and a half sequence was filtered for all 39 sites. Lemi423 also allowed access to station information such as elevation, geographic coordinates and time of deployment in GMT. Harmonics and data spikes were filtered out of data sets using a combination of low-pass filtration and elective notch filtering

through custom MATLAB applications developed by the University of Adelaide. Once

sources of noise had been removed, or reduced to the point that signal strength could

still be confidently maintained, data were decimated to 500, 100 and 25 Hz.

After decimation, all output files were converted into .EDI files using Lemigraph

software. This software offers the ability to alter dipole length, and specify the

orientation of dipoles and magnetometers if the field set up was not standard. It may

also be used to substitute magnetic coil data from neighbouring sites or a remote

reference station. The software has inbuilt robust parameters for each processing stage,

and offers the options of pre-whitening and coherence pre-sorting for further refinement

of the magnetotelluric data. In conjunction with the remote reference, if a station

produced noise-afflicted data, the magnetic data from adjacent sites was substituted to

improve resolution around the dead-band, and improve the signal-to-noise ratio.

After the above procedure, files were inverted using WinGLink geophysical modelling

software. Apparent resistivity and phase curves are able to be viewed as soundings by

using the crosspowers and autopowers to calculate each value of the resistivity and

phase. The data may then be manually refined through masking of outliers on the

resistivity or phase curves. When the data are satisfactory, they may be combined into a

single .EDI for one station, suitable for use with other geophysical software.

FIELD DATA AND MODELLING
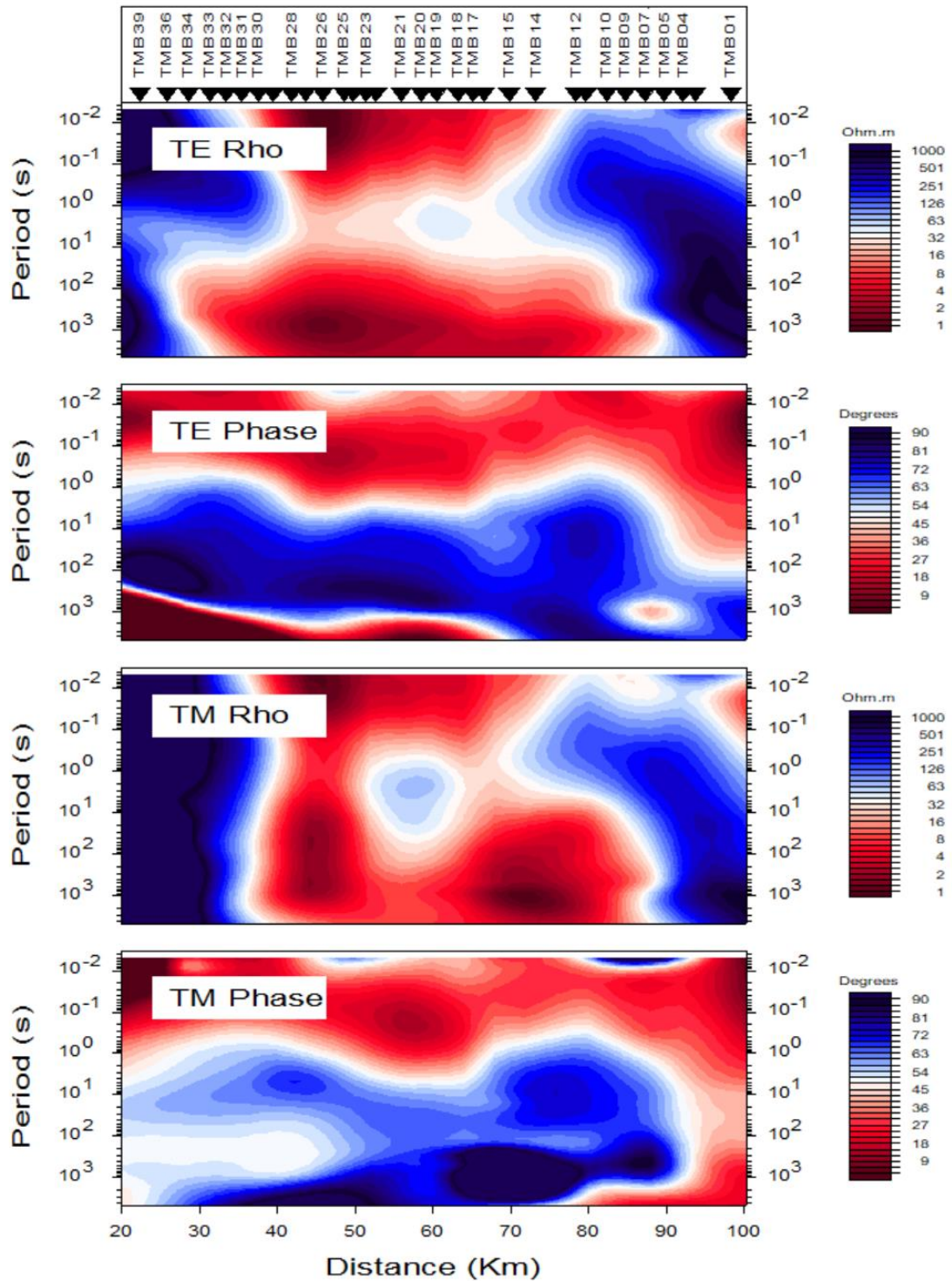
Figure 3: **Transverse electric (TE) and transverse magnetic (TM) mode pseudosections for the TB2018 transect. Rho represents the apparent resistivity, with the period reflecting the skin depth (see Appendix A: Magnetotelluric Theory). The pseudosections display the observed data as a function of the period from the 2-D model. Pseudosections were produced using WinGLink, with a site spacing of 2 km.**

The collected data were rotated 26º west of north during processing in order to align perpendicular with topography. Pseudosections indicating the observed TE and TM modes (Figure 3) were produced after data rotation. Figure 3 represents a smooth pseudosection produced for the TM and TE mods. The phase is the smoother model and more precise at identifying deeper structures, whereas the apparent resistivity is too afflicted by noise to be a reliable indicator for conductivity or resistivity features. The observable trend from east to west is that there are multiple conducting bodies, some nearer the surface, with the larger bodies deep underneath a more resistive top layer. Some station exclusions were deemed necessary where data was more affected by static shift, which can impart uncertainty into the final models produced. Data points which become anomalously 3-D as the result of noise were masked in order to fit the most precise 2-D model and pseudosections.

Modelling was also undertaken utilising MTpy, a python toolbox for magnetotelluric data processing, analysis, and visualisation developed by Geoscience Australia. These python scripts allowed for the graphical representation of the raw data in a variety of useful forms to aid the interpretation. One novel form of visualisation is phase tensors visualised as ellipses, plotted against a reference frame. The shape of the phase tensors orientation indicates the preferred direction of current flow, and demonstrates trends between stations.
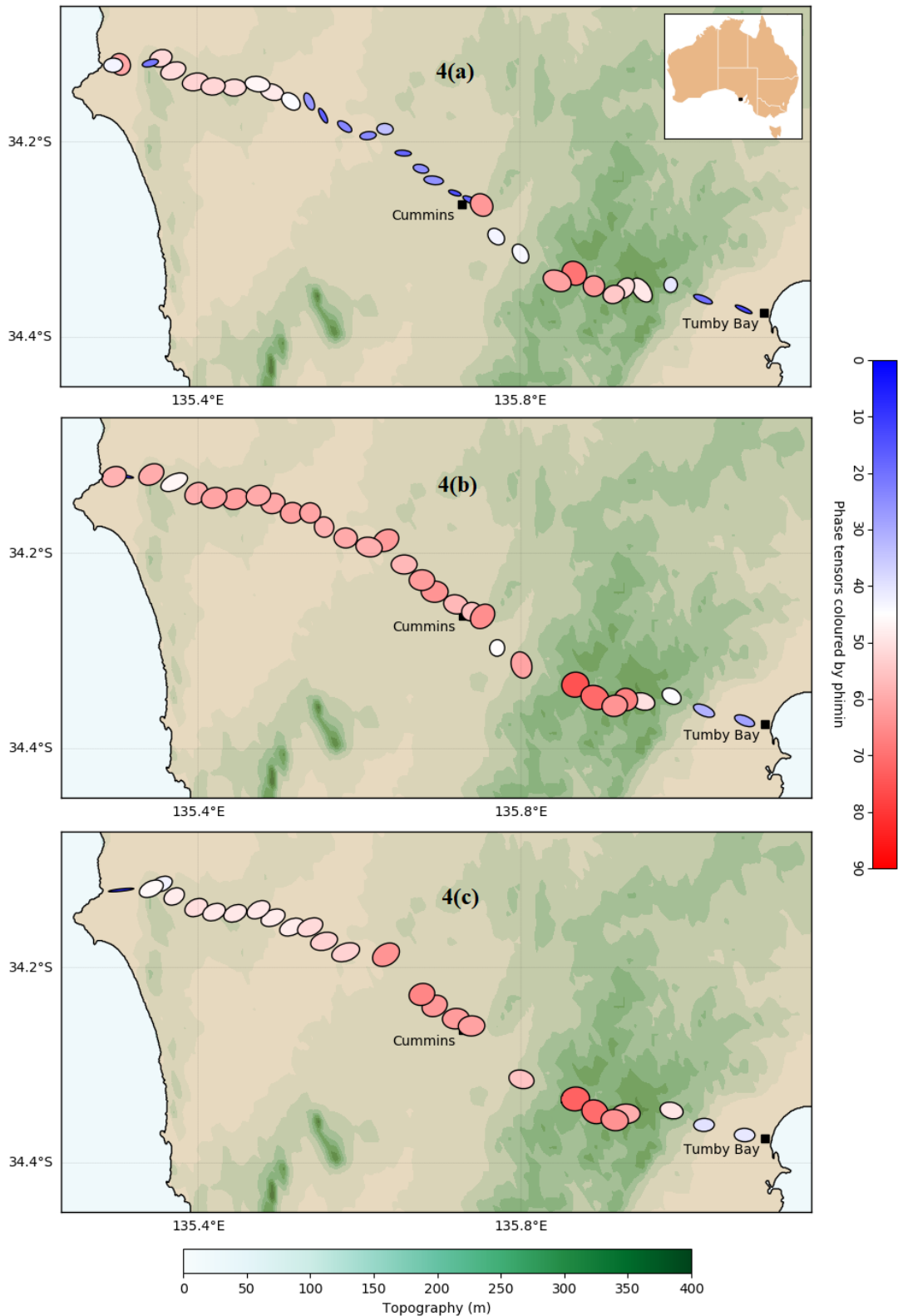
Figure 4: Phase tensor ellipses plotted against a topographic map of the southern Eyre Peninsula. The phase is plotted at ascending periods, from top to bottom: 1, 10, and 100 s (1, 0.1, and 0.01 Hz). Phase ellipses are coloured according to the minimum phase value. The basemap is plotted using topography in metres above sea level. Ellipses plotted against a basemap using MTpy

Figure 4(a) indicates phase ellipses coloured by phimin at a period of 1 s, with crustal rocks of ~10 ohm/m resistivity in the southern Eyre Peninsula (White and Polatajko, 1985; Thiel, 2005), this period corresponds to a skin depth of 0.5 km. The closest sites to Tumby Bay are becoming more resistive with depth, and the general orientation of the phase tensors shows preferred current flow towards the topographic high and the EPCA. The group of phase tensors after the KSZ are all demonstrating increasing conductivity with depth. West of these phase tensors beginning to exceed 45º are a group which are becoming increasingly resistive with depth, the orientation of preferred current flow is directed towards the EPCA. The west-most grouping is becoming more conductive with depth but to a lesser degree than the east-most group of conductivity-indicating phase tensors.

Figure 4(b) has a skin depth of 5 km, showing resistivity increasing with depth near Tumby Bay, becoming increasingly conductive with depth for the rest of the region, and most conductive at the EPCA.

Figure 4(c) has a skin depth of ~16 km and indicates the same broad regional trends as 4(a) and 4(b).

Induction arrows (Figures 1(b), 6) are another useful tool for analysing a 2-D conductivity structure, wherein the real part of the induction vector points away from the direction of increasing conductivity, thus can be reversed utilising the Parkinson convention (Parkinson, 1959), with resultant vectors pointing towards areas of heightened conductivity. The length of the arrows is determined by both the magnitude of the underlying structure, and its distance from the measurement site.

WinGLink 2-D inversion utilises the algorithm developed by Rodi and Mackie (2001). Both TE and TM modes were used to model the data over a period range between 10^{-2} to 10^{3} s. In order to undertake a smooth inversion, the data misfit and model constraint must be determined through the regularisation parameter, tau. The lower the tau value, the higher fidelity the resultant model will be; however, imprecisions can become manifest as the result of model over-development, where the higher fidelity causes issues that can exaggerate and overcorrect conductivity and resistivity structures. Therefore, a range of tau values were modelled, attempting to balance fidelity with sensibility. A tau between 5 and 20 was found to be the most reliable, and the final model utilises a tau value of 15. Phase error floors were set to 5%, and apparent resistivity error floors were set to 2.5%. The RMS for the final model was 2.21 which is close to an ideal fit of ~1.00, where less than 1.00 is a model overfit, and greater than 1.00 indicates under fit. Due to the effects of static shift and large amount of cultural noise, it was difficult to reduce the RMS to below 2.00.
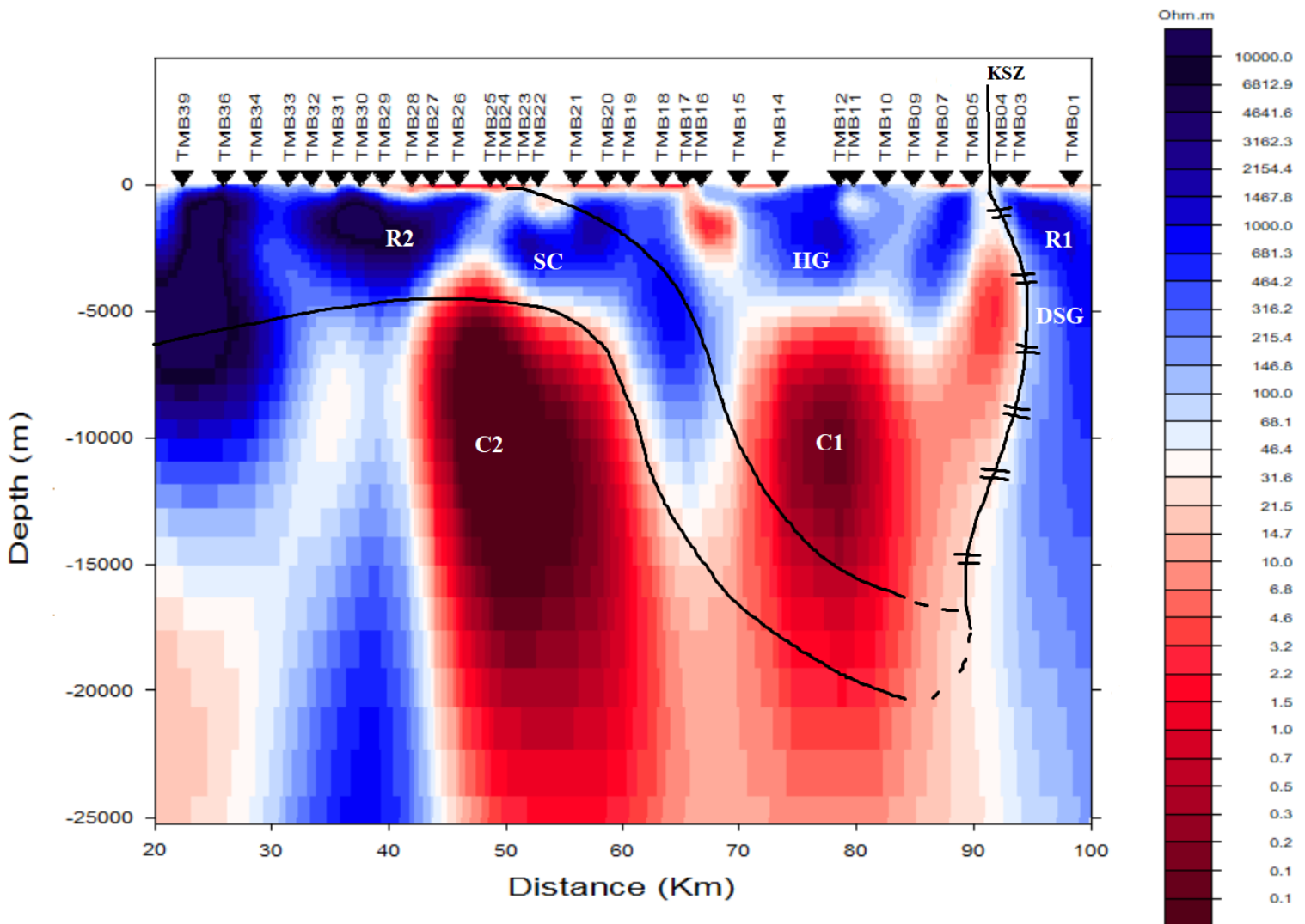
Figure 5: WinGLink 2-D inversion model of TB2018 transect, with site spacing of 2 km. C1 = 1st conductor, present at ~6 km deep, located within the Hutchison Group metasediments (HG) located between stations TMB07 and TMB15, presenting a conductivity of <0.1 ohm/m at its core. R1 = 1st resistor, located east of the Kalinjala shear zone (KSZ), and embedded in the Donington Suite granitoids (DSG), with a resistivity of 1000 ohm/m. C2 = 2nd conductor, underlying the Sleaford Complex (SC) is preserved more greatly with depth. R2 = 2nd Resistor, embedded in the Sleaford Complex, a band of very high and variable resistivity. Model RMS of 2.21, with error floors of 5% TM rho, 2.5% TM phase, 5% TE rho and 2.5% TE phase.

The 2D inversion model indicates one high conductivity zone (C1), another conductivity zone (C2) which is more extensive, more highly conducting, but less reliably constrained than C1, and two zones of resistivity surrounding the highly conductive structures (Figure 5).

The conductive top layer is not uniform, with areas TMB01 to TMB03, and TMB14 to TMB29 charting an order of magnitude more conductive than surrounding areas, and extending down ~2.5 km in close proximity to Cummins (TMB15, 16, 17). The east-most station is Tumby Bay, with a zone of high resistivity extending to ~station 4, bisected by the KSZ. East of the KSZ is the Donington Suite granitoids, containing R1 the first resistor. West of the KSZ are the Hutchison Group metasediments, C1 the first conductor is roughly arcuate, with a horizontal extent of ~10 km and a vertical extent of ~15 km, it is conductive to <0.1 ohm/m. R2 the second resistor is embedded in the Sleaford Complex basement, its resistivity exceeds 1000 ohm/m, and becomes near-vertical in the top 12 km of crust. The second conductor C2 covers a large area, beginning at 5 km depth increasing in conductive intensity towards the east and with depth. C2's resistivity gradient is extensive, ranging from ~20 to <0.1 ohm/m.

3-D modelling adds another element to our array of MT interpretation tools. The 3D forward modelling code (MTD3FWD) developed by Randy Mackie in 1999 computes magnetic and electric fields at the surface of a 3-D electrical resistivity model. One is able to input a 3-D mesh and several model parameters to produce a 3-D forward model, which automatically converts coded parameters into magnetotelluric impedances and induction vectors, which can then be converted into .EDI files for stations contained within the mesh boundaries.
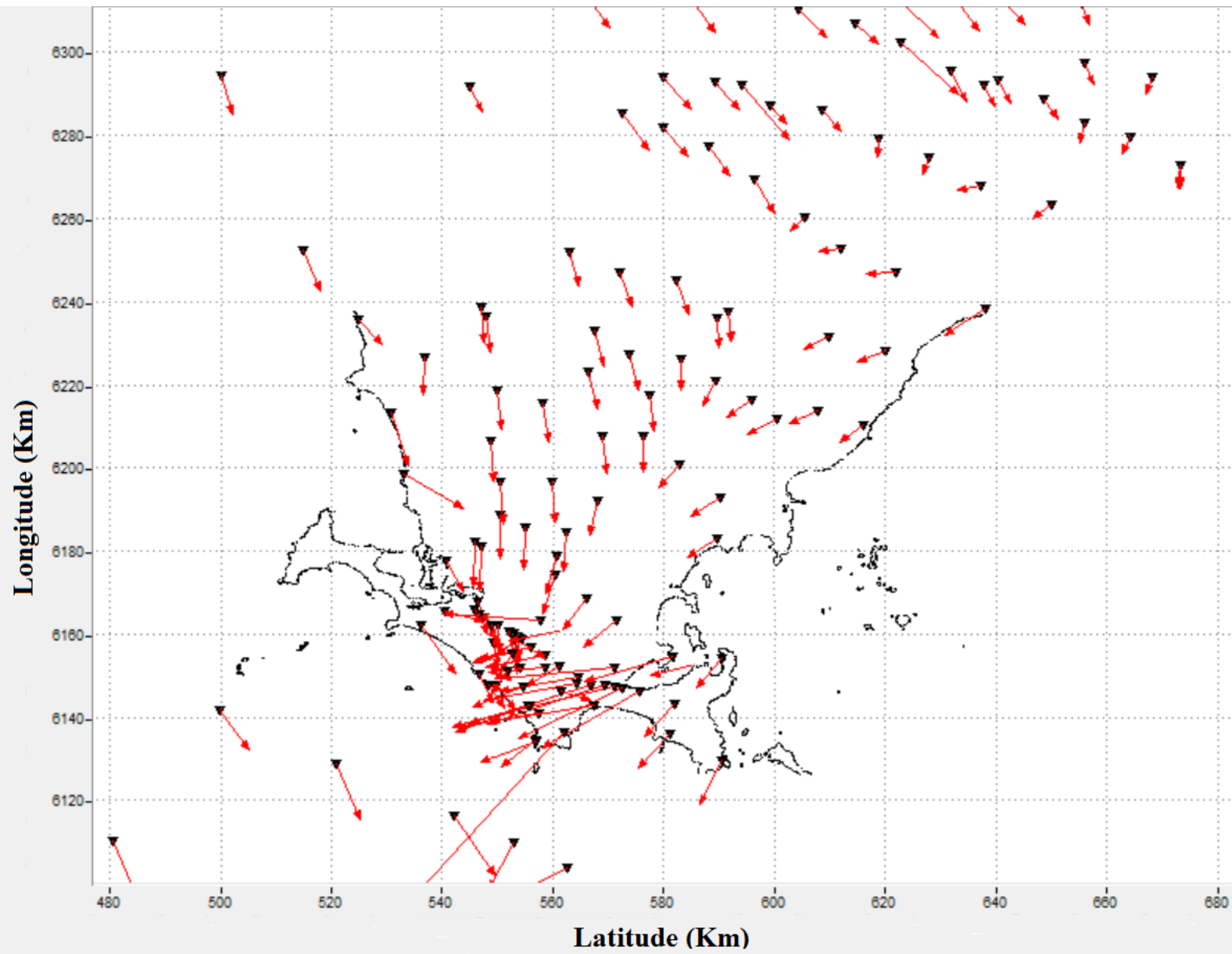
Figure 6: Parkinson induction arrow map produced from 3-D forward modelling. Each site of legacy data is indicated by an inverted black triangle. Forward model was constructed by inputting parameters from smooth 2-D inversion (Figure 5) using WinGLink 3-D forward modelling functionality.

Figure 6 was constructed by inputting the parameters from the best smooth inversion

model (Figure 5), and inferring the conductivity and resistivity features at depth slices

up to 50 km, including structural geological formations. A forward model was then

computed which output the above induction vectors.

DISCUSSION

Figures 1(b, d), 2 and 4 indicate that the EPCA is greatly aligned with topographic hills featuring the KSZ boundary on the eastern side (TMB04), and a possible reverse faulted region on the western side (TMB15). The hills occurred as a neotectonic feature, the result of east-west compression. Earthquakes associated with this compression above magnitude 4 are likewise aligned with the EPCA, predominantly on the western side, indicating that the conductor may be structurally bound by two major faults east and west.

The Eyre Peninsula conductivity anomaly is collocated with a ridge of high gravity (+ 200 to 500 mGals, Figure 1(a)). Figure 1(b) shows that induction vectors follow the gravity high zone along the EPCA, but in the north, they do not follow gravity at all. This high gravity is likely due to a mafic intrusive block of oceanic crust, compressed during the continental collision of the Kimban Orogeny, akin to the closure of the Tethys Sea to form the Himalayas (Birchfiel, 1989). The mafic intrusion plausibly formed during a period of extension as the Hutchison Group sediments were deposited, followed by rifting from shallow asthenosphere melting, concluding with a period of basin closure and sedimentary compression.

Using topography as a proxy for rheological weakness in the crust, the Kalinjala Shear Zone is a boundary between weakened and deformed Hutchison Group metasediments, and the undeformed Donington Suite granitoids. Figure 2 depicts pre and post Kimban Orogeny tectonic fabrics, with pre-Kimban fabrics being rotated through the KSZ and preserved in banded iron formations. Figure 1(c) shows the regional magnetic lineations in nanotesla, with >2000 nT magnetism occurring in line with the topographic high, gravity high, and EPCA. The banded iron formations contribute to the high density of

the Hutchison Group, alongside marble and amphibolite-facies metasediments. The density resultant from the banded iron formations may be sufficient to explain the gravity high (Figure 1(a)), however there is little regional correlation between more magnetised structures such as on the western coastline, and the gravity signatures. The gravity high is much more strongly correlated to the topography overlying the EPCA. The magnetic lineations are also unequally interspersed through the Hutchison Group, whereas the gravity readings are uniformly arrayed around the central narrow conducting band.

As the KSZ separates pre-Kimban and post-Kimban geology, it acts as a divider for changes in crustal resistivity. The Donington Suite granitoids preserve highly resistive igneous and metamorphic assemblages, forming during the Cornian Orogeny (1850 Ma) before the Kimban Orogeny deformed Hutchison Group sediments. The deformation and heat of the Kimban Orogeny instigated the graphitisation of organic-rich marine sediments, with this graphite being preserved in the fold hinges of the metamorphic rocks, producing a large conductive signature.

The proposed mechanism for graphite occurrences in the peninsula is graphitisation of organic material in 1730 Ma marine sediments, which were compressed and heated in the Kimban Orogeny. Boerner *et al*. (1996) discusses mechanisms in Palaeoproterozoic foredeeps in which under euxinic conditions, enriched organic carbon shales deposited on pre-foredeep continental margins are rendered highly conducting when graphitised by exposure to temperatures exceeding 400° C. In these scenarios, the most conductive units are located in the central hinges of the fold and thrust belt, explaining why graphite is not observed as continuous layers through the sediments. Graphite need not occur as large units to present a high conductivity at depth, Frost *et al*. (1998) reported

that very thin films of graphite (100 angstrom) can produce enhanced conductivity signatures. Graphite is present at the surface as the result of anticlinal folds, which may be faulted, shifting the entire unit to the surface. This is observed in the Middleback Subgroup as graphite is folded along the hinge of a north-plunging regional tight anticlinal fold, forming the basis for several graphite mines across the Eyre Peninsula (Keeling, 2000).

In the north-east of the region, the majority of induction arrows are broadly asymmetric, with symmetry increasing southwards, suggesting a very narrow banded conductor which broadens out in the north. The large Parkinson arrows in the south overlie Donington Suite granitoids, possessing a greater magnitude than other induction vectors due to the local resistivity contrast, as the underlying crystalline rock is very resistive, so the stations are sensitive to far away conductivity structures, such as the proposed conductivity anomaly running through the centre of the region and the conductive seawater. Seawater conductivity is a problem known as the "coast effect", resulting in real Parkinson arrows being rotated towards the coast at long periods (Chave and Jones, 2012).

The induction arrows from Figure 1(b) coupled with Figures 3 and 4 show that MT responses were predominantly 2-D over the bandwidth 100 to 0.01 Hz, with only one site exhibiting significant out of quadrant distortion, likely linked to flake graphite concentrated in the folds of near surface sediments. Figure 4 shows that phase is within 90° for nearly all the sites, demonstrating the 2-D nature of the EPCA.

The induction vectors produced from forward modelling (Figure 6) show strong agreement with those created from legacy data induction analysis (Figure 1(b)). The southern cape of the peninsula features a mass of large magnitude arrows indicating a

western conductive mass continuing off the coast, but are likely the result the coast effect given their long period and proximity to the ocean, supported by the 3-D forward model inferring bulk high conductivity for the ocean, and a very high resistivity structure emulating the Donington Suite granitoids located below these sites, outputting an array of similar-magnitude, west-pointing induction arrows. The northern arrows are broadly asymmetrical, with a lesser magnitude than is indicated by legacy data, and less alignment leading into the symmetrical central conducting band of the EPCA, suggesting the broadening conductivity band may be less diffuse than was inferred by the model. A high resistivity body (>1000 ohm/m) was constructed in the model to lie beneath conductor C1, extending below C2 and reaching its terminus west of the KSZ at a shallower depth than the Donington Suite granitoids which are modelled to extend as block of uniform resistivity, terminating at 40 km. The resistivity structure was devised as a representation of a potential mafic intrusion underlying C1, with the agreement of Figures 1(b) and 6 indicating strong evidence for the plausibility of this supposition. The very high conductivity of C2 (Figure 5) may be attributed to a large-scale strike-slip fault zone, creating a zone of fluid alteration sourced by meteoric waters percolating into a permeable zone. As crustal fluids are not well preserved over time, more considerably less well preserved at the depths C2 is located within (>5 km), it is difficult to attribute the high conductivity of C2 with crustal fluids. Another possible explanation could be sulphide occurrences, however there has been no evidence of any sulphides through the region obtained from drilling samples (Thiel, 2005). C2 is arcuate, like C1, however it is not correlated with earthquakes, topographic extremes, or gravity highs, suggesting the conductive structure of C2 did not form as a result of orogenesis. Induction arrows from Figure 1(b) and Figure 6 point away from this

conductive structure, instead of symmetrically aligning around it. While the 2-D inversion model (Figure 5) depicts it as more conducting and expansive than C1, all other evidence suggests it is most likely a flaw in the 2-D inversion parameters and station data than it is a new-found, more greatly conducting anomaly. If C2 is not located in Hutchison Group sediments, but rather a more conductive portion of the Sleaford Complex basement, a possible explanation is that the metamorphosed Carnot Gneisses of the Sleaford Complex contain small-scale fractures, or feature a grain-boundary-conducting mechanism, reducing the overall resistivity; however, this is doubtful as small-scale fractures and a grain-boundary-conducting mechanism would not be so expansive and intensely conducting without presenting evidence in surface geology.

CONCLUSIONS

The Eyre Peninsula conductivity anomaly is shallow (<6 km deep), narrow and aligned with graphite at the surface, preserving very low resistivities up to 15 km, appearing to terminate after this depth. It is collocated with a ridge of high gravity (+200 to 500 mGals), strongly aligned with topographic, neotectonic hills and correlated with earthquakes greater than magnitude 4 along its western margin. It is bound on the eastern margin by the Kalinjala Shear Zone which formed as a result of the Kimban Orogeny, and on the western margin by a plausible reverse faulted region. Induction arrows produced from legacy data sets and 3-D forward modelling symmetrically encompass the structure, and it is preserved within tightly folded late Palaeoproterozoic metasediments. In addition to this evidence, the aligned biogenic graphite at the surface and modelled resistivity of <0.1 ohm/m illustrates that the EPCA can only be the result of connected graphite networks concentrated in fold hinges, with the persistence of this connection over the last 1690 Ma likely caused by the compression and folding of Hutchison Group sediments during the Kimban Orogeny (1730-1690 Ma). The origin of the gravity high may be the result of densely layered banded iron formations; however, broader evidence suggests it is more likely caused by a large, underlying mafic intrusive block of oceanic crust, formed as a result of compression during the Kimban Orogeny. Regional maps of topography, gravity, magnetic lineations and induction arrows produced from legacy data sets were limited in the information they could impart regarding the depth and nature of the conductivity structures in the southern Eyre Peninsula, only providing clear resolution of the lateral extent of a conductivity anomaly, and its broad two-dimensionality. The densely spaced (~2 km) 39 new broadband MT sites from transect TB2018 produced an array of meaningful two-

dimensional smooth inversion models, the accuracy and agreement of which was contrasted with induction maps produced by 3-D forward modelling. The parameters of the best-fitting 2-D inversion model were input into a 3-D forward modelling algorithm, which output a new set of 226 predicted data points. The 3-D forward model induction vectors showed strong agreement with those of the legacy data, which would only be possible if the Eyre Peninsula conductivity anomaly was accurately spatially constrained by the survey.

ACKNOWLEDGMENTS

REFERENCES

BIRCHFIEL, B. C. 1989. An area of deformation: tectonic evolution of the Himalayas and Tibet. *Science*, **243**, 1221-1222.

BOERNER, D., KURTZ, R. & CRAVEN, J. 1996. Electrical conductivity and Palaeoproterozoic foredeeps. *Journal of Geophysical Research*, **101**, 13775–13789.

BRANCH, C. D. 1978. Evolution of the middle Proterozoic chandabooka caldera, Gawler Range acid volcano-plutonic province, South Australia, *Geological Society of Australia*, **25**, 199-218.

CHAVE, A., & JONES, A. 2012. *The Magnetotelluric Method*. Cambridge University Press.

FROST, B., FYFE, W., TAZAKI, K. & CHAN, T. 1989. Grain-boundary graphite in rocks and implications for high electrical conductivity in the lower crust. *Nature*, **340**, 134-136.

GAMBLE, T., GOUBAU, W. & CLARKE, J. 1979. Magnetotellurics with a remote magnetic reference. *Geophysics,* **4**, 53–68.

GILES, C. W. 1977. Rock units in the Gawler Range volcanics, Lake Everard area, South Australia. *Geological Survey of South Australia*, *Quarterly Geological Notes*, **61**, 7-16.

HAND, M., REID, A. & JAGODZINSKI, L. 2007. Tectonic framework and evolution of the Gawler Craton, southern Australia. *Economic Geology*, **102**.

JOHNS, R. K. 1961. Geology and mineral resources of southern Eyre Peninsula. *Geological Survey of South Australia*, **37**, 1-102.

KEELING, J. L. 2000. Uley graphite - a world class resource. *MESA Journal,* **18**, 6-11.

KUSI, R., WHITE, A., HEINSON, G. & MILLIGAN, P. 1998. Electromagnetic induction studies in the Eyre Peninsula, South Australia. *Geophysical Journal International*, **132**, 687–700.

MANSON, M. G., THOMSON, B. P. & TONKIN, D. G. 1978. Regional stratigraphy of the Beda Volcanics, Backy Point Beds on the southern Stuart Shelf, South Australia. *Geological Survey of South Australia*, *Quarterly Geological Notes*, **66**, 2-9.

MILLIGAN, P., WHITE, A. & CHAMALAUN, F. 1989. Extension of the Eyre Peninsula conductivity anomaly. *Exploration Geophysics*, **20**, 187–190.

PARKER, A. J. 1980. The Kalinjala mylonite zone, eastern Eyre Peninsula. *Quarterly Geological Notes, Geological survey of South Australia*, **76**, 6-11.

PARKER, A. J. 1980. Stratigraphic subdivision of the Hutchison Group on north eastern Eyre Peninsula. *Geological Society of Australia*, **27**, 45-53

PARKER, A. & LEMON, N. 1982. Reconstruction of the Early Proterozoic stratigraphy of the Gawler Craton, South Australia. *Journal of the Geological Society of Australia*, **29**, 221–238.

PARKER, A., FANNING, C., FLINT, R., MARTIN, A. & RANKIN, L. 1988. Archaean–Early Proterozoic granitoids, metasediments and mylonites of southern Eyre Peninsula, South Australia. *Geological Society of Australia Specialist Group in Tectonics and Structural Geology Field Guide 2*.

PARKER, A. J., PREISS, W. V. & RANKIN, L. R. 1993. Geological Framework. *In*: The Geology of South Australia, Volume 1 The Precambrian. *Mines and Energy of South Australia Bulletin 54* (Eds. DEXEL, J. F., PREISS, W. V. & PARKER, A. J.

PARKINSON, W. D. (1959). Direction of rapid geomagnetic fluctuations. *Geophysical Journal of the Royal Astronomical Society*, **2**, 1-14.

POPKOV, I., WHITE, A., HEINSON, G., CONSTABLE, S., MILLIGAN, P. & LILLEY, F. 2000. Electromagnetic investigation of the Eyre Peninsula conductivity anomaly. *Exploration Geophysics*, **31**, 187–191.

RODI, W. & MACKIE, R. 2001. Nonlinear conjugate gradients algorithm for 2-D magnetotelluric inversion. *Geophysics*, **66**, 174–187.

RUTLAND, R. W. R., PARKER, A. J., PITT, G. M., PREISS W. V. & MURRELL, B. 1981. "The Precambrian of South Australia. *In*: HUNTER, D. R. (Ed.), Precambrian of the Southern Hemisphere. *Developments in Precambrian Geology*, **2**, 309-360.

SCHWARZ, M. 2002. Lincoln Map Sheet, sheet SH53 – 11. Geological Atlas 1:250 000. Office of Minerals and Energy of South Australia, Adelaide.

SPRIGG, R. C. 1952. Sedimentation in the Adelaide Geocyncline and the formation of the continental terrace. *In*: GLAESSNER, M. F. and SPRIGG, R. C. (Eds.), *Sir Douglas Mawson Anniversary Volume. University of Adelaide*, 153-159.

THIEL, S., HEINSON, G. & WHITE, A. 2005. Tectonic evolution of the southern Gawler Craton, South Australia, from electromagnetic sounding. *Australian Journal of Earth Sciences* **52**, 887-896.

THOMSON, B. P. 1980. Roopena stratigraphic diamond drillholes 1 and 1A. South Australia. *Department of Mines and Energy*. Report Book, 80/147.

VASSALLO, J. J. & WILSON, C. J. L. 2002. Palaeoproterozoic regional-scale non-coaxial deformation: an example from eastern Eyre Peninsula, South Australia. *Journal of Structural Geology*, **24**, 1–24.

VEEVERS, J. J. 1986. Breakup of Australia and Antarctica estimated as mid-cretaceous (955 Ma) from magnetic and seismic data at the continental marfgin. *Earth and Planetary Science Letters*, **77**, 91-99.

WEBB, A. W., THOMSON, B. P., BLISSETT, A. N., DAY, S. J., FLINT, R. B. & PARKER A. J. 1986. Geochronology of the Gawler Craton, South Australia. *Journal of Earth Sciences*, **33**, 119-143.

WHITE, A. & HOPGOOD, D. N. 1979. The island and coast effect in geomagnetic variations around St. Vincent's Gulf, South Australia. *Journal Geomagnetism and Geoelectricity,* **31**, 479-484.

WHITE, A. & MILLIGAN, P. 1984. A crustal conductor on Eyre Peninsula, South Australia. *Nature*, **310**, 219–222.

WHITE, A. & MILLIGAN, P. 1986. Geomagnetic variation anomaly on Eyre Peninsula South Australia. *Exploration Geophysics*, **17**, 32–34.

WHITE, A. & POLATAJKO, O. 1985. Electrical Conductivity Anomalies and their Relationship with the tectonics of South Australia. *Geophysical Journal of the Royal Astronomical Society*, **80**, 757-771.

APPENDIX A: MAGNETOTELLURIC THEORY

In order to understand the electromagnetic field within a material of a static frame of reference, one must observe Maxwell's equations. An electric field is induced in the time-varying magnetic field within the medium. The basis of the magnetotelluric method relies on the following four equations, expressed in differential form as:

$$\nabla \times E \equiv -\left(\frac{\partial B}{\partial t}\right)$$

$$\nabla \times H = J + \left(\frac{\partial D}{\partial t}\right)$$

$$\nabla \cdot D = \rho$$

$$\nabla \cdot B = 0$$

Where E represents the electric field, [V/m];
H represents the magnetic field, [A/m];
B represents the magnetic induction, [T];
D represents the electric displacement current, [C/m^2];
J represents electric current density, [A/m^2];
ρ represents electrical charge density of free charges, [C/m^3].

Natural variations in the induced electric fields and native magnetic fields occur over periods between 10^{-3} to 10^5 s. The range of frequencies between 0.5 to 5 Hz is qualified as the dead-band range, over which MT responses generally suffer low quality due to the low intensity of natural electromagnetic fluctuations. To resolve the earth's crust, broadband magnetotellurics of a period range between 10^{-3} and 10^3 s may be taken. The earth's conductive structure, coupled with the electromagnetic sounding period determine the penetration depth of MT signals. Signals penetrate at approximately one skin depth, where an electromagnetic field is attenuated to 1/e of its initial amplitude at the surface. In a uniform material, this depth is a function of resistivity and frequency of the subsurface, and is described by the following;
$$\delta(T) \approx 500\sqrt{T\rho_a} \,,$$
where ρ_a is the resistivity of the structure. The investigation depth is determined by the penetration depth, increasing along with the square root of the period and material resistivity. Despite a reliance on homogeneous media, equation (skin depth) is able to be applied to real geological structures.

IMPEDANCE TENSOR

Natural fluctuations of electric (E) and magnetic fields (H) are described by complex impedances in the frequency domain. The impedance tensor Z is defined as:
$$\begin{pmatrix} E_x \\ E_y \end{pmatrix} = \begin{pmatrix} z_{xx} & z_{xy} \\ z_{yx} & z_{yy} \end{pmatrix} \begin{pmatrix} H_x \\ H_y \end{pmatrix},$$
where x indicates the north-south direction, and y is the east-west direction. The earth's resistivity (ρ) is described by the complex impedance tensor Z, with the solution to magnetotelluric problems simplified to resistivity reconstructions from the frequency

dependence of Z. Information about vertical variations in the conducting structure are acquired from the off-diagonal components of Z. There are three ways to classify the spatial distribution of resistivity:

In a one-dimensional resistivity structure, the diagonal components of resistivity variations with depth are able to be summarised as;

$$z_{xy} = -z_{yx} = z, z_{xx} = z_{yy} = 0,$$

with the impedance tensor being written as;

$$Z = \begin{pmatrix} 0 & z_{yx} \\ z_{yx} & 0 \end{pmatrix}, z_{yx} \neq z_{xy}.$$

For a two-dimensional structure, resistivity varies in one direction laterally with depth, remaining constant in the horizontal direction. The impedance tensor in a 2D resistivity structure is able to be rotated to an angle which defines the geo-electric strike, eliminating Zxx and Zyy. Zxy is hence referred to as the transverse electric (TE) mode, with the electric field parallel to strike; correspondingly, Zyx is referred to as the transverse magnetic (TM) mode, with the magnetic field parallel to strike. The requirement of the 2-D scenario is that |Zyx| and |Zxy| are not equal.

In the three-dimensional earth as resistivity varies in all three directions, it follows that the impedance tensor becomes;

$$Z = |\begin{matrix} Z_{xx} & Z_{xy} \\ Z_{yx} & Z_{yy} \end{matrix}|,$$

where Zxx =/= Zyy =/= 0 and Zxy =/= Zyx. In a 3D structure, associated EM fields are unable to be resolved into the distinct polarisations.

Apparent resistivity expresses the magnitude of the magnetotelluric impedance at frequency (ω) through the expression;

$$\rho_{a_{ij}}(\omega) = \frac{1}{\mu_0 \omega} |z_{ij}(\omega)|^2.$$

Apparent resistivity represents a weighted average of signals over the penetration depth, equal to the resistivity of a half-space possessing the same response at the measured point. The impedance phase and apparent resistivity are common terms used to specify the magnetotelluric response. The phase response indicates the conductivity gradient with depth at the penetration depth. When the phase exceeds 45° it is an indication that conductivity is increasing with depth, conversely a phase less than 45° indicates conductivity decreasing with depth. In 1-D and 2-D structures, the phase will lie between the range of 0° and 90°, with some 3-D structures possessing a phase in this range also. Phase exceeding 90° is indicative of increasing dimensionality. The phase, used to calculate the MT impedance is expressed as;

$$\phi_{ij} = \tan^{-1}(\frac{\Im(Z_{ij})}{\Re(Z_{ij})})$$

Pseudosections are a means of presenting phase responses and apparent resistivity, comprised of site locations along the horizontal axis, with period on the vertical axis and phase and apparent resistivity indicated by contours.

INCLUDING A REMOTE REFERENCE STATION
Magnetotelluric data is susceptible to cultural noise present nearby or at the survey site. This noise may come from a nearby road, inhabited areas of various density, proximity to a mobile transmission tower, even cathodic protection on water pipelines can be a

highly affecting source of noise. Gamble *et al*. (1979) suggested a method of locating an MT station in an area free of as many sources of noise as possible, a reference station from which clean magnetic data can be accessed and transplanted to noise-afflicted sites. During processing, the apparent resistivity data curve may be biased down due to noise in the magnetic field. A remote reference station is able to provide better quality data during processing, and a higher signal to noise ratio.

PHASE TENSOR THEORY

Before data is inverted, it is important to analyse the phase tensor which for a 2-D regional conductivity structure is symmetric with one of its principal axes aligned parallel to its strike axis. For a 2-D case, the coordinate invariants of the phase tensor (its principal values) are the magnetic polarization and transverse electric phases. In both 2-D and 3-D situations, the components of the impedance tensor can be used to orient the principal axes of the phase tensor. The phase tensor is represented by;

$$\phi = X^{-1}Y.$$

Where X is the real component, and Y the imaginary component of Z.

A valuable factor in the analysis of resistivity data is the geoelectric strike, which is useful for delineating the faults and fractures at various depths, which make ideal channels for crustal fluids. It is calculated as the preferred direction of current flow, given as either a or $a + 90$ to account for the variation between principal axes (Caldwell *et al.*, 2004), and represented as;

$$a = \frac{1}{2}\tan^{-1}\frac{\phi_{xy} + \phi_{yx}}{\phi_{xx} - \phi_{yy}}$$

As a structure becomes more 3-D than 2-D, the phase tensor becomes asymmetrical, with the asymmetry of the regional MT response being measured by the skew (β), where;

$$\beta = \frac{1}{2}\tan^{-1}\frac{\phi_{xy} - \phi_{yx}}{\phi_{xx} + \phi_{yy}}$$

The phase tensor is able to be graphically represented as an ellipse (Caldwell *et al.*, 2004), giving an indication of strike direction and data dimensionality. The axes of the ellipse represent the principal axes of the phase tensor. Lateral variations in the regional resistivity structure are replicated in the orientations of the phase tensor principal axes.

THE EFFECT OF STATIC SHIFT

Telluric, or static shift problems affect the magnetotelluric method, which measures a surface electric field. Small, near-surface inhomogeneities create static shift, which appears as a vertical shifting of the apparent resistivity curve, independent of frequency, with no change in the phase curve (Chave & Jones, 2012). (Jiracek 1990) proposed that resistive inhomogeneities in the vicinity of the electrical dipoles caused the shift. While this is a contributing factor, the voltage distortion of the electric field can more completely be attributed to topographic distortion, conductive minerals, and current channelling.

GEOMAGNETIC DEPTH SOUNDING

A magnetic field is comprised of both vertical and horizontal components (H_x, H_y, H_z), a method for measuring these components was developed in 1889 by Schuster and Lamb upon their discovery of induced magnetovariational fields. Given the exclusion

of electric fields in geomagnetic depth sounding (GDS), the process is not influenced by local electrical distortions which create galvanic distortion (Bibby *et al.* 2005) and static shift (Jones, 1988). GDS is extensive, probing both lateral and vertical lengths, detecting lateral resistivity variations for hundreds of kilometres. It is limited by its inability to determine absolute resistivity values, and needs to be supplemented by magnetotelluric methods to more precisely resolve vertical depths. The magnetic field transfer function is defined by;

$$(H_z) = \begin{pmatrix} T_{xz} \\ T_{yz} \end{pmatrix} \begin{pmatrix} H_x \\ H_y \end{pmatrix}.$$

Where the vertical transfer function is represented by the induction vector, $\vec{K}$, defined as;

$$H_z = -\vec{K} \cdot H.$$

MT STRIKE ANALYSIS

As the diagonal elements of the impedance tensor are minimised, the electrical strike reflects information about their direction. Geological fractures often align with these directions, while the strike direction rarely coincides with the layout of the measurements. The impedance tensor allows one to perform a two-dimensional analysis of magnetotelluric data, by rotating the tensor by an angle (alpha symbol). The angle the tensor makes with geographical north is the Swift angle (Swift, 1967). The impedance of the 3-D earth can be approximated closely to the 2-D model via rotation of the impedance tensor by the angle (alpha symbol). By using the skew parameter, we can determine the dimensionality of the structure, expressed by;

$$S = \begin{bmatrix} Z_{xx} & + & Z_{yy} \\ Z_{xy} & - & Z_{yx} \end{bmatrix}.$$

For a 1-D earth, the skew parameter is zero; for 2-D, the parameter should approach zero after rotation of the impedance tensor; and in the 3-D earth, the skew indicates the dimensionality of the subsurface structure.

APPENDIX A: MAGNETOTELLURIC THEORY REFERENCES:

SWIFT, C. M. (1967). A magnetotelluric investigation of an electric conductivity anomaly in the south-western U.S. PhD thesis, Massachusetts Institute of Technology, Cambridge.

JIRACEK, G. R. (1990). Near-surface and topographic distortion in electromagnetic induction. *Surveys in Geophysics*, **11**, 163–203.

JONES, A. G. 1988. Static shift of magnetotelluric data and its removal in a sedimentary basin environment, **53**, 967-978.

CALDWELL, T. G., BIBBEY, H. M. & BROWN, C. 2004. The magnetotelluric phase tensor. *Geophysical Journal International*, **158**, 457-469.

GAMBLE, T., GOUBAU, W. & CLARKE, J. 1979. Magnetotellurics with a remote magnetic reference. *Geophysics,* **4**, 53–68.

BIBBY, H. M., CALDWELL, T. G., and BROWN, C. (2005). Determinable and nondeterminable parameters of galvanic distortion in magnetotellurics. *Geophysical Journal International*, **163**, 915-930.

APPENDIX B: SITE STATION INFORMATION

Site Name	Date & Time (UTC)	Lat	Long	Elevation
TMB01	18/07/18 23:38:13	-34' 22.27488	136' 04.63921	7.9
TMB02	19/07/18 01:52:19	-34' 21.39552	136' 03.24610	34.6
TMB03	21/07/18 01:05:32	-34' 21.65385	136' 01.61980	62.9
TMB04	21/07/18 06:45:15	-34' 21.57840	136' 00.47934	130.9
TMB05	19/07/18 02:04:50	-34' 20.76765	135' 59.21003	187.5
TMB06	21/07/18 02:58:22	-34' 21.14963	135' 58.61673	206.4
TMB07	18/07/18 23:54:14	-34' 21.09342	135' 57.06090	306.1
TMB08	19/07/18 03:20:33	-34' 20.97221	135' 55.81790	251.3
TMB09	19/07/18 04:21:04	-34' 21.35768	135' 54.97947	261.3
TMB10	21/07/18 04:18:56	-34' 20.84766	135' 53.50765	194.5
TMB11	20/07/18 05:06:48	-34' 20.05959	135' 52.04765	207.5
TMB12	20/07/18 03:43:15	-34' 20.52400	135' 50.77094	222.8
TMB13	20/07/18 02:32:25	-34' 19.48963	135' 49.82515	144.8
TMB14	21/07/18 02:44:50	-34' 18.85296	135' 48.04521	120.9
TMB15	20/07/18 05:31:09	-34' 17.80412	135' 46.23698	85.1
TMB16	20/07/18 04:06:37	-34' 15.86427	135' 45.15216	87.5
TMB17	20/07/18 02:30:08	-34' 15.57317	135' 45.33267	69.8
TMB18	21/07/18 01:15:24	-34' 15.12550	135' 43.16050	56.5
TMB19	22/07/18 04:17:29	-34' 14.34500	135' 41.58650	66.6
TMB20	22/07/18 03:23:02	-34' 13.63400	135' 40.64000	63.6
TMB21	22/07/18 02:31:22	-34' 12.67266	135' 39.31833	66
TMB22	22/07/18 03:42:34	-34' 11.19200	135' 37.96916	54
TMB23	22/07/18 02:24:43	-34' 11.59900	135' 36.70567	50
TMB24	22/07/18 01:26:19	-34' 11.22900	135' 35.72400	49.3
TMB25	24/07/18 02:27:14	-34' 11.04100	135' 34.96967	41
TMB26	23/07/18 01:15:34	-34' 10.36947	135' 33.36418	37.7
TMB27	23/07/18 02:19:43	-34' 09.49800	135' 32.32933	42
TMB28	24/07/18 01:41:38	-34' 09.49157	135' 30.96283	34
TMB29	23/07/18 03:00:59	-34' 08.91800	135' 29.56683	45
TMB30	23/07/18 02:16:05	-34' 08.42400	135' 28.48216	51
TMB31	23/07/18 03:09:41	-34' 08.64503	135' 26.75073	108.3
TMB32	24/07/18 00:55:32	-34' 08.57000	135' 25.18111	102.6
TMB33	18/07/18 05:41:41	-34' 08.29094	135' 23.85426	92.2
TMB34	18/07/18 03:54:36	-34' 07.60948	135' 22.21739	65.6
TMB35	18/07/18 01:07:00	-34' 06.83708	135' 21.29536	59.5
TMB36	18/07/18 02:36:47	-34' 07.13334	135' 20.51418	101.3
TMB37	18/07/18 04:31:00	-34' 07.10124	135' 19.23884	28.8
TMB38	18/07/18 05:39:59	-34' 07.21015	135' 18.27243	4.6
TMB39	22/07/18 01:20:05	-34' 06.83628	135' 17.74898	57.5

Table A.1: Table of sites along transect TB2018, indicating each station's date and time of deployment, its geographic location and the elevation in metres above sea level.
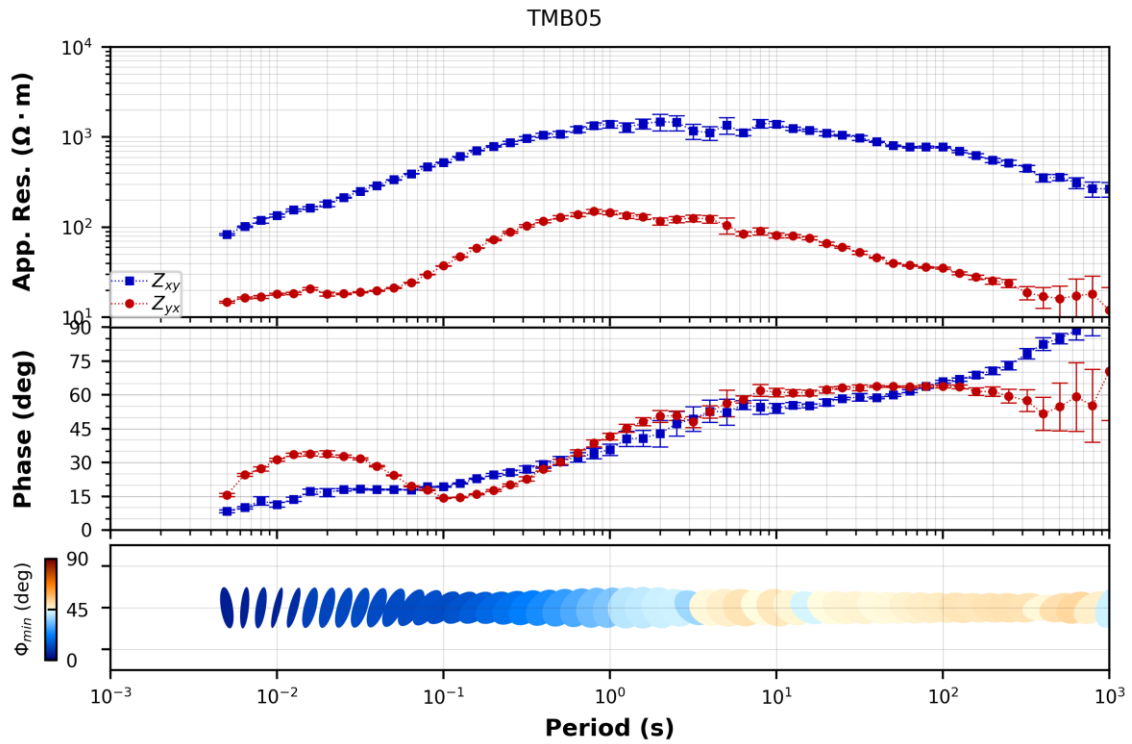
Figure A.1: Processed MT data for sounding TMB05 from the southern Eyre Peninsula TB2018 broadband survey. The top graph is the apparent resistivity, below this is the phase angle. The phase angle is expressed at the bottom as phase tensors coloured by phimin. All measurements are a function of Period. The phase range for this station presents the site's 2-dimensionality, with the phase never exceeding 90º at any point.
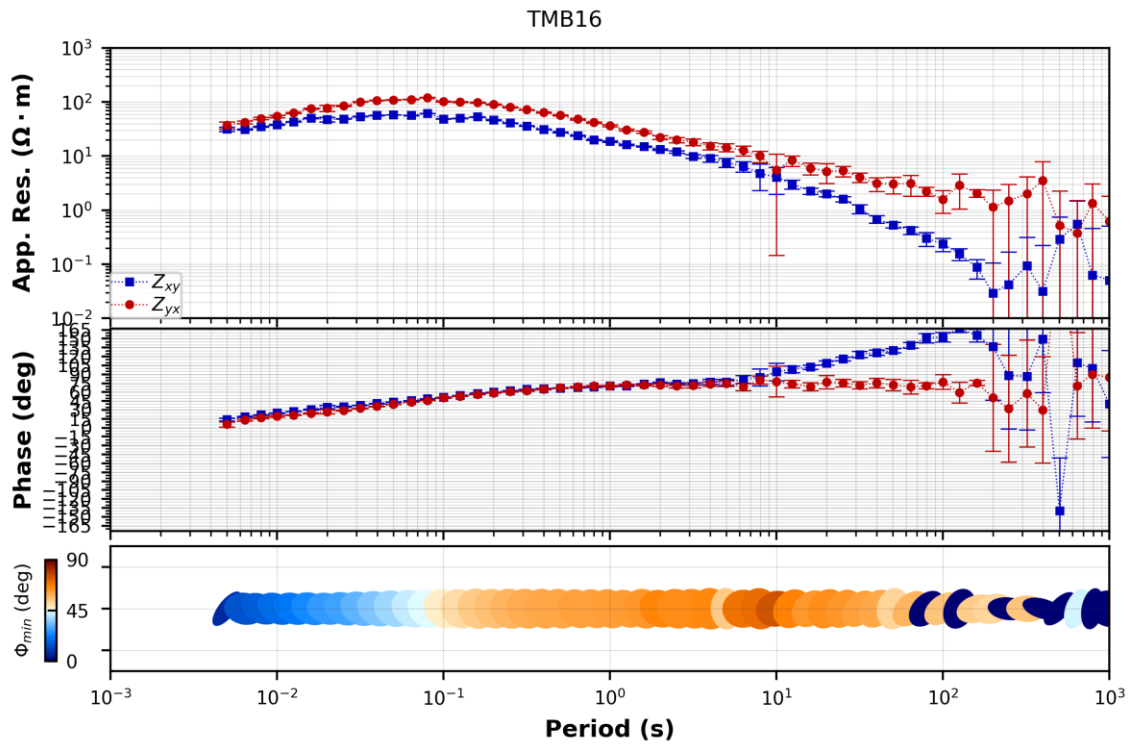
Figure A.2: Processed MT data for sounding TMB16 from the southern Eyre Peninsula TB2018 broadband survey. The top graph is the apparent resistivity, below this is the phase angle. The phase angle is expressed at the bottom as phase tensors coloured by phimin. All measurements are a function of Period. The phase range for this station presents the site's 3-dimensionality, with the phase exceeding 90º at periods above 10 s.